

Boggart: Accelerating Retrospective Video Analytics via Model-Agnostic Ingest Processing

Neil Agarwal, Ravi Netravali
Princeton University

Abstract

Delivering fast responses to retrospective queries on video datasets is difficult due to the large number of frames to consider and the high costs of running convolutional neural networks (CNNs) on each one. A natural solution is to perform a subset of the necessary computations ahead of time, as video is *ingested*. However, existing ingest-time systems require knowledge of the specific CNN that will be used in future queries – a challenging requisite given the evergrowing space of CNN architectures and training datasets/methodologies.

This paper presents Boggart, a retrospective video analytics system that delivers ingest-time speedups in a model-agnostic manner. Our underlying insight is that traditional computer vision (CV) algorithms are capable of performing computations that can be used to accelerate diverse queries with wide-ranging CNNs. Building on this, at ingest-time, Boggart carefully employs a variety of motion tracking algorithms to identify potential objects and their trajectories across frames. Then, at query-time, Boggart uses several novel techniques to collect the smallest sample of CNN results required to meet the target accuracy: (1) a clustering strategy to efficiently unearth the inevitable discrepancies between CV- and CNN-generated outputs, and (2) a set of accuracy-preserving propagation techniques to safely extend sampled results along each trajectory. Across many videos, CNNs, and queries Boggart consistently meets accuracy targets while using CNNs sparingly (on 3-54% of frames).

1 INTRODUCTION

Video cameras are prevalent in our society, with massive deployments across major cities and within individual organizations [2, 4, 5, 11]. These cameras continually collect video data, which is then stored and queried “after-the-fact,” or *retrospectively*. Example use cases include traffic planning, business analytics, and law enforcement [3, 12, 15, 16, 38].

The main goals of retrospective video analytics pipelines are to deliver query results with high accuracy and low latency. However, simultaneously achieving these goals is difficult given the potentially massive number of video frames to consider, and the expensive convolutional neural networks (CNNs) commonly used for vision processing tasks such as classification or detection [30, 70, 73, 75, 88]. For example, recent object detectors run at 3-10 frames per second (fps) on modern GPUs, with additional speedups coming only with accuracy degradations [50, 54]—this translates to 500 GPU-hours to process a week of 30-fps video from one camera.

Given the practical importance of retrospective video analytics, much work has been expended to improve query response times [21, 53, 64–66]. The prevailing (and most effective)

acceleration technique is to perform certain computations ahead of time, as video is ingested (i.e., at *ingest-time*), and then to use the outputs to speed up response generation once a query is issued (at *query-time*). More specifically, at ingest-time, existing systems cluster similar objects [53] or frames [66] using specialized or compressed CNNs that approximate the full CNN used at query-time by generating comprehensive but imprecise results.¹ Then, at query-time, these systems run the full CNN only on a subset of frames in each cluster (e.g., centroids), and quickly propagate the results to the remaining frames to improve precision.

Unfortunately, despite their performance benefits, existing ingest-time approaches face two primary drawbacks with regards to generalization in retrospective scenarios.

- First, and foremost, they all assume *a priori* (i.e., at ingest time) knowledge of the specific CNN(s) that will be used at query-time. Meeting this assumption is impractical in retrospective pipelines where queries can be made at any point in the future, users often supply their own CNNs [18, 20, 22, 23, 44, 55], and the space of potential CNNs is immense, with variations in architecture (e.g., # of layers, neurons) or weights (e.g., different datasets, including proprietary ones). Yet, we find that performing ingest work with a different CNN (architecture- or weight-wise) than that used at query-time can result in accuracy degradations of up to 94% (§2.3). Avoiding such accuracy drops by performing ingest tasks for all possible CNNs would be prohibitively expensive: tasks scale with the number of CNNs to consider, and must be repeated as that set evolves. Other systems [21, 65] sidestep these issues by training specialized models at query-time (when the CNN is known), but in doing so, forego the potential speedups of running computations ahead of time.
- Second, all prior ingest-time systems can directly accelerate queries based on object presence (e.g., binary classification), but not object location (e.g., bounding box detections); the latter are sped up via indirect binary classification, with the CNN running on all frames containing the object(s) of interest. This omission is fundamental, since bounding box queries require new and more precise forms of result propagation, and also crucial, as detections fuel numerous applications, e.g., those that involve object tracking [25, 89] or inter-object spatial relationships [76].

To address these issues, we built **Boggart**, a retrospective video analytics system that delivers ingest-time speedups in a

¹ Compressed CNNs are used in place of the full one to lower resource costs, especially given the potential for wastage (if the query is never made).

model-agnostic manner and for a wide range of query types. In designing Boggart, we make three primary contributions.

Identifying (useful) model-agnostic ingest-time tasks. The driving insight behind Boggart is that, if applied properly, traditional computer vision (CV) algorithms [29, 60, 71, 87, 91] – i.e., those that characterize video data, not any given CNN’s perception of it – can comprehensively perform much of the heavy lifting in response generation for both presence-based and location-based queries. More specifically, Boggart’s ingest-time phase extracts a set of *potential* objects (or blobs) in each frame, as well as the *trajectories* of those blobs across frames. Blob bounding boxes are extracted as areas of motion relative to the background scene, while trajectories are computed by tracking low-level, model-agnostic video features (e.g., keypoints from SIFT [78]). Model-specific tasks such as the classification of blobs (and their trajectories) are deferred until query-time. Importantly, trajectories are a key enabler to Boggart’s model-agnostic speedups. Indeed, compared to the clustering on CNN features that prior systems use to enable cross-frame result propagation, Boggart’s trajectories provide an alternate way of linking information across frames, but can be computed without knowledge of the CNN that will be used.

Quickly adapting to user queries. At query-time, Boggart takes a user CNN, and aims to generate results for all frames as quickly as possible, while adhering to the target accuracy. In its simplest form, this entails running the CNN on the minimum set of frames such that all trajectories appear at least once; results (e.g., the label for a blob) could then be propagated along each trajectory to account for the remaining frames. Unfortunately, (1) CNNs can produce inconsistent results for the same object across frames [68], and (2) even for consistent results, propagation errors can build to unacceptable levels over long trajectories. The implication is that propagating a single result across each trajectory may be insufficient to meet the accuracy target, and the CNN should be run on additional frames to sufficiently bound the effects of these issues. To efficiently identify the smallest set of additional frames to consider, Boggart leverages our observation that the above issues are largely determined by model-agnostic features about the target video (e.g., scene dynamics). Building on this, Boggart divides the video into chunks, clusters the chunks according to those features, and runs the CNN only on each cluster’s centroid chunk to determine the appropriate frame selection strategy for the rest of the cluster.

Handling errors in CV algorithms. The primary difficulty in propagating CNN results across frames pertains to the fact that Boggart’s CV-derived ingest-time outputs are coarse and imprecise relative to CNN results. For instance, blob bounding boxes may be far larger than the corresponding CNN-generated bounding box, and may include multiple objects that move in tandem. Worse, the discrepancies (e.g., coordinate transformations for bounding boxes) between these

outputs vary across frames. To cope with this, Boggart introduces a set of accuracy-preserving result propagation techniques that are specific to each query type, and explicitly consider both the information that must be propagated, as well as the required precision. Most notably, for bounding box detections (which prior systems do not support), we find that the relative position between an object’s model-agnostic keypoints (from ingest-time) and its bounding box edges remain stable over time. Accordingly, Boggart propagates each CNN-generated bounding box along the corresponding trajectory by efficiently searching for the coordinates on each frame that maximally preserve these spatial relationships.

We evaluated Boggart using 96 hours of video from 8 public camera feeds, a variety of CNNs and accuracy targets, and three query types (for people and cars): binary classification, counting, and bounding box detection. Overall, Boggart consistently meets accuracy targets while running the CNN on only 3-54% of frames. Further, Boggart (1) outperforms query-time systems (NoScope [65]) by 38-94% and, (2) compared to systems that perform *model-specific* ingest processing (Focus [53]), has 58% lower ingest costs and response times that are 56% (15%) lower for detections (counting), and only 11% higher for classification.

2 BACKGROUND AND MOTIVATION

We begin with an overview of retrospective video analytics pipelines (§2.1). We then discuss existing optimizations (§2.2), and present measurements that highlight their inability to generalize to different query types and models (§2.3).

2.1 Overview on Retrospective Video Analytics

In a typical retrospective video analytics workflow, live video is first generated by a camera (or cameras) and streamed to a server where it is ingested, potentially processed for live analytics or in preparation for later (retrospective) analysis, and then stored. Users may issue questions about stored video at any point in the future, by specifying a query to run, an accuracy target for the result, and a subset of the video to consider (e.g., a time range). The goal of these pipelines is to provide query results on each frame as fast as possible, while ensuring that the average result accuracy meets the user’s target.

Queries typically involve convolutional neural networks (CNNs), a class of deep neural networks that represent the state-of-the-art for vision processing. CNNs can support a variety of query types, with common ones being [74, 79]:

- **binary classification:** return a binary decision as to whether a specific object or type of object appears in each frame. Accuracy is measured as the fraction of frames tagged with the correct binary value.
- **counting:** return the number of objects of a given type that appear in each frame. Per-frame accuracy is set to the percent difference between the returned and correct counts.
- **bounding box detection:** return the coordinates for the bounding boxes that encapsulate each instance of a spe-

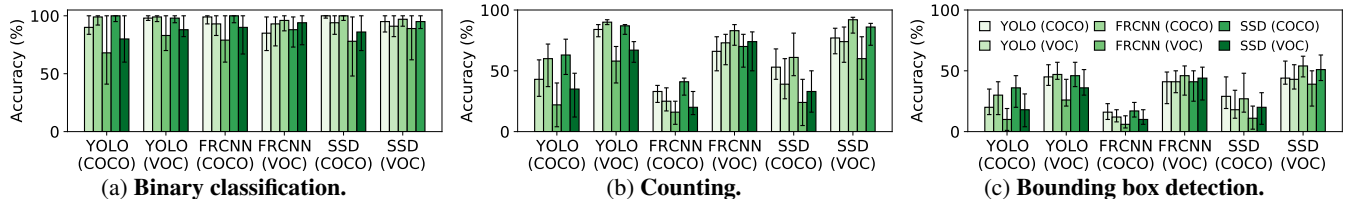


Figure 1: Query accuracies when *different* CNNs are used for ingest-time (bar types) and query-time (X axes). Bars show results for the median video, and error bars span the 25-75th percentiles. Models are listed as ‘architecture (training dataset)’.

cific object or object type in each frame. Accuracy for each frame is measured using the standard mAP score [42], which considers the overlap (intersection over union, or IOU) of each returned bounding box with the correct one.

2.2 Existing Acceleration Approaches

Existing optimizations for retrospective video analytics can be classified into two categories: query-time and ingest-time. We describe them next and discuss other related work in §7.

Query-time strategies. Systems such as NoScope [65] and Tahoma [21] only operate once a user issues a query. To accelerate the response process, they first train cascades of cheaper binary classification CNNs that are specialized to the object of interest and video being considered. The specific cascade to use is selected with the goal of meeting the accuracy target while minimizing computation and data loading costs. If confidence is lacking with regards to meeting the accuracy target, the user-provided CNN is incrementally run on frames until sufficient confidence is achieved.

Ingest-time strategies. Other systems provide speedups by shifting certain query processing tasks to ingest-time, i.e., when the video is stored and before the query is even made. For example, Focus [53] accelerates binary classification queries by building an approximate index of all object occurrences using a specialized and compressed CNN that roughly matches the user-specified CNN on the target video; in other words, the cheaper model is used to collect comprehensive (i.e., high recall) but imprecise results relative to the user CNN. Objects are then clustered based on the features extracted by the compressed model such that, at query-time, the user’s CNN only runs on the centroid of each cluster, with labels being propagated to all other objects in the same cluster, i.e., to improve precision of the ingest-time results.

BlazeIt [64] and TASTI [66] accelerate aggregate versions of certain query types, e.g., total counts across all frames. TASTI uses sampled results from the user’s CNN to train a cheap embedding CNN that runs on all frames and clusters those that are similar from the model’s perspective. At query-time, the user’s CNN is run only on representative frames in each cluster, with the results propagated to the rest. In contrast, BlazeIt generates sampled results from the user’s CNN at ingest-time. At query-time, BlazeIt uses those results to train specialized CNNs that act as control variates for the remaining frames: the specialized CNNs run on all frames, and

the results are correlated with sampled results from the user’s CNN to provide guarantees in statistical confidence.

2.3 The Problem: Lack of Ingest-Time Generalization

Conceptually, ingest-time strategies can deliver superior speedups as they shield users from the delays of certain processing tasks. Query-time approaches forego this opportunity, and instead perform all work in a blocking manner, including the training to develop optimizations and the (accelerated) query processing. Prior work [53] and our results in §6.3 confirm the relative performance of these approaches.

Unfortunately, despite their potential, all existing ingest-time systems suffer from two main drawbacks with respect to generalization (§1). First, whereas they directly accelerate binary classifications, and by simple extension counting queries, existing systems provide limited acceleration for the bounding box detection queries that many applications rely on [25, 33, 46, 76, 89, 102]. In particular, prior systems do not support cross-frame result propagation for bounding boxes, and instead are restricted to acceleration via binary classification, i.e., the CNN must be run on all frames containing the object of interest. This omission is fundamental since detections pose strict accuracy requirements, and rely not just on object presence, but also on precise object location.

Second, and more importantly, these systems all assume a priori (i.e., at ingest-time) knowledge of the exact CNN that a user will provide for a future query. In particular, knowledge of the user CNN is required to train the specialized/compressed models that Focus uses to build approximate indexes, and to collect sampled results for BlazeIt and TASTI. This is an unrealistic expectation for retrospective analytics where users often specify the specific CNNs to use for their queries by selecting from the massive landscape of potential models that cover numerous architectures and weights.

To quantify the impact of this assumption, we ran experiments to answer the following question: how would accuracy be affected if the user’s model at query-time was different (architecturally or weight-wise) than the model used to perform ingest-time work? Our experiments considered the three query types described above, the objects of interest and videos described in §6.1, and a wide range of models. More specifically, we considered three popular architectures—Faster RCNN, YOLOv3, and SSD—each trained on two widely used datasets: COCO and VOC Pascal.

For each possible pair of ingest- and query-time models,

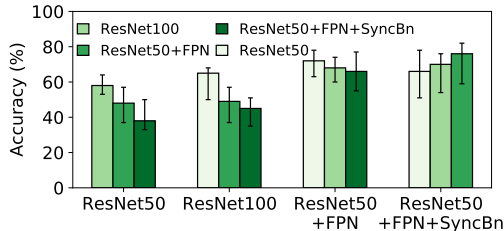


Figure 2: **Accuracies when ingest- (bar types) and query-time (X axis) CNNs are FasterRCNN+COCO versions with different ResNet backbones. Results are for counting queries; bars list medians with error bars for 25-75th percentiles.**

we ran both models on the video to obtain a list of object bounding boxes. In line with Focus’ observation that classification results from two models may not identically match but should intersect for the top- k results [53], we ignore the classifications from each model. Instead, we consider all ingest-time bounding boxes that have an IOU of ≥ 0.5 with some box generated by the query-time model; results were largely unchanged for different IOU thresholds. This presents the best scenario (accuracy-wise) for existing ingest-time strategies and is akin to setting k to its maximum possible value with Focus. Moreover, ignoring classification results is helpful since our two datasets are labeled with different levels of object specificity, e.g., a car in VOC may be classified as a truck in the more precise COCO dataset. Finally, we compute query results separately using only the remaining ingest-time boxes or all of the query-time boxes, and compare the results.

Figure 1 shows that discrepancies between ingest- and query-time models can lead to significant accuracy degradations, with the errors growing as query precision increases. For example, median degradations were 0-32% for binary classifications, but jump to 8-84% and 46-94% for counting and detections. Parsed differently, median degradations across query types were 0-84%, 2-94%, and 1-90% when the ingest- and query-time CNNs diverged in terms of only architecture, only weights, or both. Figure 2 shows that these degradations persist even for model variants in the same family. Such errors are unacceptable given the stringent accuracy goals that users specify (typically $\geq 90\%$) [53, 63, 74].

3 OVERVIEW OF BOGGART

This section presents a high-level overview of the workflow that Boggart employs to (1) perform ingest-time processing tasks that generalize to different models, and (2) leverage the outputs to speed up a variety of query types (at query-time) while adhering to the specified accuracy targets. Figure 3 illustrates Boggart’s end-to-end operation, and we detail its ingest- and query-time functionality in §4 and §5.

Ingest-time. As input, Boggart’s ingest-time module takes video(s) that are either already stored or currently streaming in to a cloud or edge server; note that Boggart does not optimize video transmission or storage, and focuses entirely on video from *static cameras*. From there, Boggart’s overarch-

ing goal is to maximally process the video such that the outputs can enable the sparing use of the user’s CNN at query-time. However, to sidestep the pitfalls of prior approaches that share this strategy (§2.3), Boggart introduces a novel set of ingest-time tasks that are model-agnostic (i.e., they do not incorporate any knowledge of the specific query-time CNNs) and can accelerate a range of query types. Importantly, this means that ingest-time work must only be performed once per video, and the outputs can be safely (accuracy-wise) used to accelerate queries with different CNNs.

Our underlying insight is that traditional computer vision (CV) algorithms [29, 60, 71, 87, 91] are well-suited for such ingest-time work, as they extract information purely about the video data, rather than how a specific model or query would parse that data. Further, they can be configured to extract comprehensive information about the video, leaving the CNN only to filter out unnecessary results and correct the remaining ones (at query-time). Accordingly, Boggart uses a combination of motion extraction and low-level feature tracking techniques to identify potential objects as areas of motion (or *blobs*) relative to a background estimate, and record their *trajectories* across frames by tracking each blob’s defining pixels (or keypoints). Static objects are left to be quickly discovered at query-time via CNN sampling.

Trajectories represent a fundamental shift from the clustering strategies that prior systems use to group frames or objects based on how they are perceived by the query-time CNN (§2.2). In contrast, trajectories are computed in a model-agnostic manner, but still provide a mechanism through which to propagate CNN results across frames at query-time – the primary source of speedups. Such generality does, however, come at a cost. Whereas prior efforts cluster on entire frames or object classes, Boggart’s trajectories group frames on a per-object basis. This discrepancy lets Boggart defer the determination of how a CNN perceives each object to query-time, but it limits the amount of potential result propagation, i.e., Boggart propagates the result for an object across the frames in which it appears, while prior approaches could propagate results across the appearances of different objects. Note that this discrepancy applies only to binary classification; bounding box detections require precise location information, so results cannot be propagated purely based on cross-object feature similarity.

A natural question is: why not cluster objects on the features extracted by traditional CV algorithms to enable more result propagation? The issue is that, if performed without knowledge of the query-time CNN, such clustering could lead to unsafe result propagation. More specifically, objects that are similar on some set of features but are perceived differently by the query-time CNN could end up in the same cluster. For instance, cars of different brands may end up in the same cluster depending on the considered features, but result propagation across those objects would not be safe if the CNN was (say) only searching for cars of one brand.

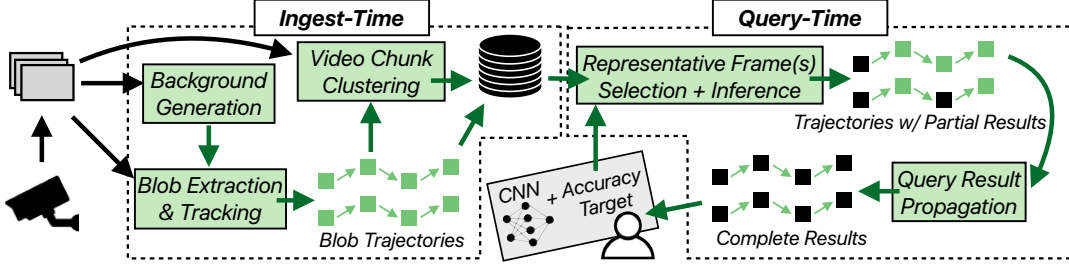


Figure 3: Overview of Boggart.

Query-time. At query-time, users provide a CNN (of any composition), a query type, an accuracy target, and a range of video to consider. Boggart’s goal is to generate a complete set of per-frame results as quickly as possible, while adhering to the target accuracy. This translates to running the CNN on a small sample of frames, and then using the outputs from ingest-time (i.e., blobs and trajectories) to efficiently propagate those sampled CNN results to the remaining frames.

The overarching challenge is that, despite their generality to different models and queries, the CV algorithms used at ingest-time operate on low-level, noisy signals and produce results that fail to precisely align with those from the CNN [74]. These errors are dictated by the interaction between video properties (e.g., scene dynamism) and CNN operation, build up as results are propagated across longer durations, and are unstable across an object’s trajectory. Running the CNN on additional frames can mitigate the associated accuracy degradations, but at the cost of performance.

To resolve this tension, Boggart employs two new ideas. First, to efficiently unearth discrepancies between CNN and ingest-time outputs, Boggart clusters chunks of video using video properties that capture the aforementioned effects (e.g., dynamics, trajectory lengths). Boggart then runs the CNN only on the cluster centroids to determine the best frame selection strategy per cluster, i.e., the frequency of frames to run the CNN on. Note that clustering technically occurs at ingest-time since it does not rely on the CNN.

Second, Boggart introduces a set of accuracy-preserving propagation techniques that are specific to each query type and address the instability in CV errors. Most notably, for bounding box detections, Boggart leverages our empirical observation that the relative position between an object’s keypoints (from ingest-time) and its bounding box edges remain stable over time. Building on this, Boggart propagates an object’s CNN-produced bounding box to subsequent frames in its trajectory by efficiently searching for the coordinates that maximally preserve these spatial relationships.

4 MODEL-AGNOSTIC INGEST PROCESSING

Boggart’s target output at ingest-time is a set of blobs and their trajectories. To efficiently extract this information, Boggart operates independently on chunks (contiguous frames) of the video being considered. This yields two benefits: (1) Boggart can process chunks in parallel to leverage the avail-

able compute resources, and (2) Boggart can operate on stored or streaming video. Boggart’s default chunk size is 1 min; we profile this parameter in §6.4. The rest of this section describes the analysis that Boggart performs per chunk.

Background generation. Extracting blobs inherently requires a point of reference against which to discern areas of motion. Thus, Boggart’s first task is to generate an estimate of the background scene for the current chunk. However, state-of-the-art background estimation approaches [24, 72] are ill-suited for use in Boggart as they are primarily concerned with generating a single, coherent background image despite scene dynamics (e.g., motion) that complicate perfect foreground-background separation. In contrast, Boggart’s focus is on navigating the following tradeoff between accuracy and efficiency, not coherence. On the one hand, placing truly background pixels in the foreground will lead to spurious trajectories (and query-time inefficiencies). On the other hand, incorrectly placing a temporarily static object in the background can result in accuracy degradations. Indeed, unlike entirely static objects that will surely be detected at query-time via CNN sampling and can be safely propagated to all frames in a chunk, temporarily static objects may be missed and should only be propagated to select frames.

Boggart addresses the above tradeoff in a manner that favors accuracy. More specifically, Boggart only marks content as pertaining to the background scene when it has high confidence; all other content is conservatively marked as part of the foreground and is resolved at query-time. To realize this approach, Boggart eschews recent background estimation approaches in favor of a custom, lightweight strategy.

In its most basic form, background estimation involves recording the distribution of values assigned to each pixel (or region) across all frames in the chunk, and then marking the most frequently occurring value(s) (i.e., the peaks in the probability density function) as the background [87, 91]. This works well in scenarios where there is a clear peak in the distribution that accounts for most of the values, e.g., if objects do not pass through the pixel or do so with continuous motion, or if an object is entirely static and can thus be safely marked as the background. However, complications arise in settings with multiple peaks. For instance, consider a pixel with two peaks. Any combination of peaks could pertain to the background: a tree could sway back and forth (both), a

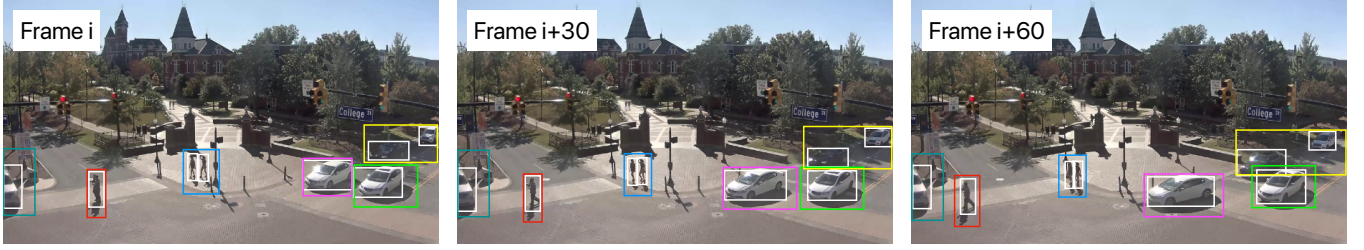


Figure 4: Example screenshots from the Auburn video (Table 1). CNN (YOLOv3+COCO) detections are shown in white, while each of Boggart’s trajectories (and their constituent blobs) is shown in a different color.

single car could temporarily stop at a traffic light (one), or multiple cars could serially stop-and-go at the light (none).

To distinguish between these multi-modal cases and identify peaks that definitely pertain to the background for a chunk, Boggart extends (into the next chunk) the duration over which the distribution of pixel values is computed. The idea is that motion amongst background components should persist (i.e., in our example, two peaks should remain) as we consider more video, while cases with temporarily static object should steadily transform into uni-modal distributions favoring either the background scene or the object (if it remains static). To distinguish between the object and background in the latter case, Boggart further extends the distribution of pixel values to incorporate video from the previous chunk. If the same peak continues to rise, it must pertain to the background since we know that the object was not static throughout the entire chunk. Otherwise, Boggart conservatively assigns an empty background for that pixel.

Note that the above approach is not used to compute the background over a longer duration, and instead is solely designed to differentiate between multi-modal scenarios. The reason is that gradual content changes (e.g., due to lighting) are more pronounced over long durations, resulting in pixels unnecessarily marked as foreground (harming efficiency).

Blob Extraction. Using the background estimate, Boggart takes a second pass through the chunk in order to extract areas of motion (blobs) on each frame. More specifically, Boggart segments each frame into a binary image whereby each pixel is annotated with a marker specifying whether it is in the foreground or background. Our implementation deems a pixel whose value falls within 5% of its counterpart(s) in the background estimate as a background pixel, but we find our results to be largely insensitive to this parameter. Given the noise in low-level pixel values [74], Boggart further refines the binary image using a series of morphological operations [81], e.g., to convert outliers in regions that are predominantly either background or foreground. Lastly, Boggart derives blobs by identifying components of connected foreground pixels [45], and assigning a bounding box using the top left and bottom right coordinates of each component.

Computing Trajectories. Boggart’s final ingest-time task is to convert the set of per-frame blobs into trajectories that track each blob across the video chunk. At first glance, it

may appear that multi-object trackers [27, 97] could directly perform this task. However, most existing trackers rely on pristine object detections as input. In comparison, blobs are far coarser and imprecise (Figure 4). At any time, a single blob may contain multiple objects, e.g., two people walking together. Blobs may split or merge as their constituent objects move and intersect. Lastly, the dimensions of a given object’s blob bounding boxes can drastically fluctuate across frames based on interactions with the estimated background. Taken together, the issue is that we need to track the contents of each blob, but those contents can vary over time.

To handle these issues, we turn to tracking algorithms that incorporate low-level feature keypoints (SIFT [78] keypoints in particular) [60, 61], or pixels of potential interest in an image, e.g., the corners that *may* pertain to the windshield of a car. Associated with each keypoint is a descriptor that incorporates information about its surrounding region, and thus enables the keypoint (and its associated content) to be matched across images. Boggart uses this functionality to generate correspondences between blobs across frames. In more detail, for each pair of consecutive frames, Boggart pairs the constituent keypoints of each blob. This may yield any form of an $N \rightarrow N$ correspondence depending on the underlying tracking event, e.g., blobs entering/leaving a scene, fusion or splitting of blobs. For instance, if the keypoints in a blob on frame f_i match with keypoints in N different blobs on frame f_{i+1} , there exists a $1 \rightarrow N$ correspondence.

To generate trajectories, Boggart makes a series of forwards and backwards scans through the chunk. For each correspondence that is not $1 \rightarrow 1$, Boggart propagates that information backwards to account for the observed merging or splitting. For example, in the event of a $1 \rightarrow N$ correspondence between frames f_i and f_{i+1} , Boggart would split frame f_i ’s blob into N components using the relative positions of the matched keypoints on frame f_{i+1} as a guide. §5 describes how Boggart conservatively handles any remaining tracking errors to consistently meet its accuracy targets (§6). We note that Boggart’s efficiency will also inherently benefit from the steady improvements in tracking [99].

5 FAST, ACCURATE QUERY-TIME PROCESSING

At query-time, Boggart’s sole goal is to judiciously use the user-provided CNN and the outputs from ingest-time to

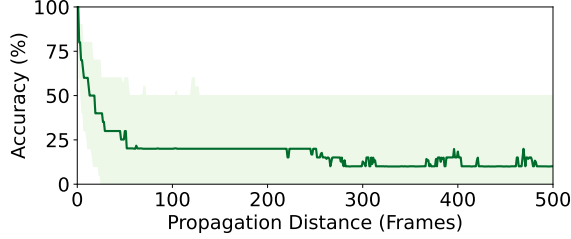


Figure 5: Accuracy (mAP) degradations when CNN bounding boxes are propagated by computing the blob-to-detection coordinate transformation on a representative frame, and applying it to all other blobs in the trajectory. Line represents median detections, with ribbons spanning 25-75th percentiles.

quickly generate a complete set of results that meet the specified accuracy target. Doing so involves answering two questions: (1) what sampled (or *representative*) frames should the CNN be run on such that we can sufficiently adapt to the provided query (i.e., CNN, query type, and accuracy target) and address ingest-time imprecisions?, and (2) how can we use the ingest-time outputs to accurately propagate sampled CNN results across frames for different query types? For ease of disposition, we describe (2) first, assuming CNN results on representative frames are already collected.

5.1 Propagating CNN Results

Regardless of the query type, Boggart’s first task is to pair the CNN’s bounding box detections on representative frames with the blobs on those same frames; this, in turn, associates detections with trajectories, and enables cross-frame result propagation. To do this, we pair each detection bounding box with the blob that exhibits the maximum, non-zero intersection. Trajectories that are not assigned to any detection are deemed spurious and are discarded. Further, detections with no matching blobs are marked as ‘entirely static objects’ and are handled after all other result propagation (described below). Note that, with this approach and in spite of the trajectory corrections from §4, multiple detections could be associated to a single blob, i.e., when objects move together and never separate. Using these associations, Boggart propagates CNN results via techniques specific to the target query type.

Binary classification and counting. To support both query types, each trajectory is labeled with an object count according to the number of detections associated with it on representative frames. If a trajectory passes through multiple representative frames, Boggart partitions the trajectory into segments, and assigns each segment a count based on the associations from the closest representative frame. Lastly, Boggart sums the counts across the trajectories that pass through each frame, and returns either the raw count (for counting), or a boolean indicating if count > 0 (for binary classification).

Bounding box detections. Whereas binary classification and count queries simply require propagating coarse information about object presence, bounding box queries require precise positional information to be shared across frames.

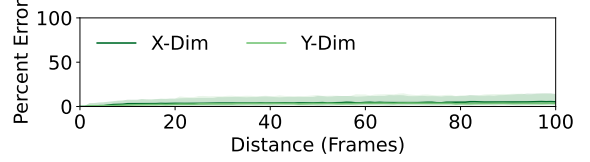


Figure 6: Percent difference in anchor ratios for each object’s keypoints across its trajectory. Line shows medians, with ribbons spanning 25-75th percentiles.

However, as noted in §4, blobs and trajectories are inherently imprecise and fail to perfectly align with detections. A natural approach to addressing such discrepancies is to compute coordinate transformations between paired detections and blobs on representative frames, and apply those transformations to the remainder of each blob’s trajectory; equivalently, one could compute transformations for a blob across its own trajectory, and apply them to add detections to non-representative frames. Unfortunately, Figure 5 shows that detection accuracy rapidly degrades with this approach, e.g., median degradations are 30% when propagating a box over 30 frames. The reason is that blobs and their paired detections move/resize differently across frames, resulting in median errors of 84% between the Euclidean distances of blob-blob and detection-detection coordinate transformations.

To fill the void of stable propagation mechanisms, Boggart leverages our finding that the relative positions between an object’s constituent keypoints (i.e., interesting points, e.g., corners, as per §4) and its (detection) bounding box edges remain largely unchanged over short durations; we refer to these relative positions as *anchor ratios* since they ‘anchor’ an object’s content to a relative position within the bounding box. This stability is illustrated in Figure 6, and is intuitive: objects tend to remain rigid over short time scales, implying that the points they are composed of move in much the same way as the entire object does (including as the object scales in size). Building on this, Boggart propagates detections by finding matching keypoints along the trajectories to which they have been associated, and efficiently solving an optimization problem in search of bounding box coordinates that maximally preserve the anchor ratios for each keypoint. Note that keypoints are extracted and tracked for trajectory construction at ingest-time, and simply reused at query-time.

More formally, for each detection on each representative frame, Boggart considers the set of keypoints K that fall in the intersection with the associated blob (since these were tracked at ingest-time). Each keypoint k in K has coordinates (x_k, y_k) . Further, let the coordinates of the detection bounding box be (x_1, y_1, x_2, y_2) , where (x_1, y_1) refers to the top left corner and (x_2, y_2) refers to bottom right corner. Then, the anchor ratios for keypoint k , or (ax_k, ay_k) , are computed as:

$$(ax_k, ay_k) = \left(\frac{x_2 - x_k}{x_2 - x_1}, \frac{y_2 - y_k}{y_2 - y_1} \right) \quad (1)$$

For each subsequent non-representative frame (until the next

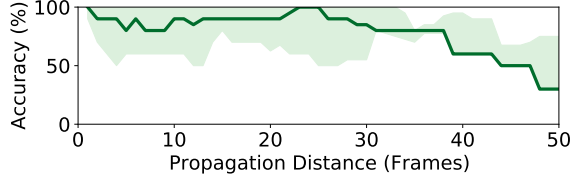


Figure 7: **Accuracy (mAP) degradations grow as Boggart propagates detection bounding boxes over longer durations. Results consider all object trajectories in the median video. Line represents medians, with ribbons for 25-75th percentiles.**

representative frame) that includes the same trajectory, Boggart finds the set of keypoints that match with those in K ; denote the set of matching keypoints as K' , where each k' in K' matches with keypoint k in K . Finally, to place the bounding box on the subsequent frame, Boggart solves for the corresponding coordinates (x_1, y_1, x_2, y_2) by minimizing the following function to maximally preserve anchor ratios:

$$\sum_{k'}^{K'} \left[\left(\frac{x_2 - x_{k'}}{x_2 - x_1} - ax_k \right)^2 + \left(\frac{y_2 - y_{k'}}{y_2 - y_1} - ay_k \right)^2 \right] \quad (2)$$

Note that this optimization (which takes 1 ms for the median detection) can be performed in parallel across frames and across detections on the same frame. Further, Boggart initializes each search with the coordinates of the corresponding detection box on the representative frame, thereby reducing the number of steps to reach a minima.

Propagating entirely static objects. Thus far, we have only discussed how to propagate detection bounding boxes that map to a blob/trajectory, i.e., moving objects. However, recall from §4 that certain objects which are entirely static will be folded into the background scene. These objects are discovered by the CNN on representative frames, but they will not be paired with any blob. Instead, Boggart broadcasts these objects to nearby frames (until the next representative frame) in a query-specific manner: such objects directly add to the per-frame counts used for binary classification and count queries, and are statically added to frames for bounding box queries (in the positions that they were detected).

5.2 Selecting Representative Frames

In order to utilize the result propagation techniques from §5.1, we must determine the set of sampled, representative frames to collect CNN results on. Importantly, because CNN execution is the largest contributor to query-time delays (§6.4), our goal is to select the smallest set of representative frames such that Boggart can sufficiently discern the relationship between ingest-time outputs and CNN results, and generate a complete set of accurate results.

Since trajectories are model- and query-agnostic, and Boggart’s result propagation only occurs within each trajectory, a natural strategy for selecting representative frames is to pick the smallest set of frames such that every trajectory appears at least once. In theory, executing the CNN on this

set of frames should be sufficient to generate a result (e.g., object label, bounding box) for each trajectory, and propagate that result to all of the trajectory’s frames. However, this straightforward approach falls short for two reasons:

1. CNNs can be inconsistent and occasionally produce different classification labels for the same object across frames, e.g., a car in frame i may be ignored in frame $i + 1$ [68,69]. We mostly observe this behavior for small or distant (and thus, small in the scene) objects. This follows from prior analyses that report lower-accuracy CNN results for smaller objects, e.g., YOLOv3 mAP scores are 18% and 42% for the small and large objects in the COCO dataset [84]. The consequence is that, if such an inconsistent result appears on a representative frame, Boggart would propagate it to all other frames in the trajectory, thereby spreading the error.
2. Even for consistent CNN results, propagation errors inherently grow with longer trajectory lengths (i.e., as a given result is propagated to more frames). For instance, median accuracies are 90% and 30% when Boggart propagates bounding boxes over 10 and 50 frames (Figure 7).

These issues are more pronounced in busy/dynamic scenes with significant object occlusions/overlap [52, 95]. Moreover, the implication of both is that solely ensuring that the set of representative frames covers each trajectory is insufficient and can result in unacceptable accuracy degradations. To address this, Boggart introduces an additional constraint to the selection of representative frames: any blob in a trajectory must be within *max_distance* frames of a representative frame that contains the same trajectory. This, in turn, bounds both the duration over which inconsistent CNN results can be propagated, as well as the magnitude of propagation errors.

Tying back to our original goal, we seek the largest *max_distance* (and thus, smallest set of representative frames) that allows Boggart to meet the specified accuracy target. However, the appropriate *max_distance* depends on how the above issues manifest with the current query type, CNN, and video. Digging deeper, we require an understanding of how Boggart’s propagation techniques (for the query type at hand) and the user’s CNN interact with each video frame and trajectory, i.e., how accurate are Boggart’s propagated results compared to the ground truth CNN results. Though important for ensuring sufficient accuracy, collecting this data (particularly the CNN results) for each frame at query-time would forego all of Boggart’s speedups.

To achieve both accuracy and efficiency, Boggart clusters video chunks based on properties of the video and ingest-time data that characterize the aforementioned issues (i.e., CNN inconsistencies and propagation errors). The idea is that the chunks in each resulting cluster should exhibit similar interactions with the CNN and Boggart’s result propagation, and thus should require similar *max_distance* values. Accordingly, Boggart could determine the appropriate

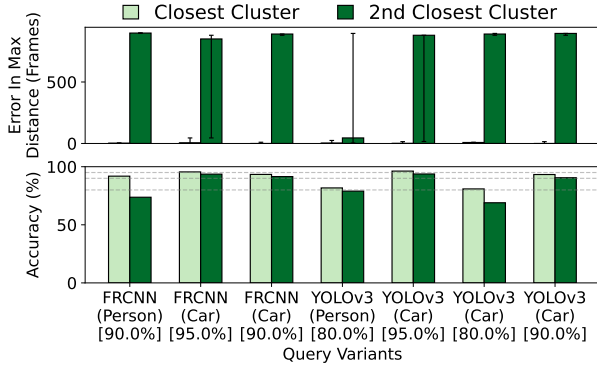


Figure 8: **Effectiveness of Boggart’s clustering with different CNNs, (object types), and [accuracy targets]. Results are for the median video, and compare the ideal $max_distance$ value for each chunk with those of the centroids in its cluster and the nearest neighboring cluster. The top graph measures the discrepancies in per-chunk $max_distance$ (bars list medians, with error bars for 25-75th percentile); the bottom graph evaluates the corresponding hits on average accuracy (for detections).**

$max_distance$ for all chunks in a cluster by running the CNN and result propagation only on the cluster’s centroid chunk.

To realize this clustering approach, for each video chunk, Boggart extracts distributions of the following features: object sizes (i.e., pixel area per blob), trajectory lengths (i.e., number of frames), and busyness (i.e., number of blobs per frame, number of trajectory intersections). These features match our observations above: CNN inconsistencies are most abundant in frames with small objects, the potential for propagation errors is largest with long trajectories, and both issues are exacerbated in busy scenes. Note that Boggart performs feature extraction and clustering at ingest-time since none of these features depend on the CNN; we present the clustering approach here for ease of disposition.

With these features, Boggart clusters chunks using the K-means algorithm. We find that setting the number of target clusters to ensure that the centroids cover 2% of video strikes the best balance between CNN overheads and robustness to diverse and rapidly-changing video chunks; we profile this parameter in §6.4. For each resulting cluster, Boggart runs the CNN on all frames in the centroid chunk. Using the collected results, Boggart runs its result propagation for a range of possible $max_distance$ values, and computes an achieved accuracy for each one relative to the ground truth CNN results. More precisely, for each $max_distance$, Boggart selects the specific set of representative frames to run the CNN on by greedily adding frames until all blobs satisfy our requirement (i.e., all blobs are within $max_distance$ frames of the closest representative frame containing the same trajectory). From there, Boggart selects the largest $max_distance$ that meets the specified accuracy goal, and applies it to pick representative frames for all other chunks in the same cluster.

Figure 8 highlights the effectiveness of Boggart’s cluster-

Camera location	Resolution
Auburn, AL (University crosswalk + intersection) [6]	1920 × 1080
Atlantic City, NJ (Boardwalk) [13]	1920 × 1080
Jackson Hole, WY (Crosswalk + intersection) [8]	1920 × 1080
Lausanne, CH (Street + sidewalk) [9]	1280 × 720
Calgary, CA (Street + sidewalk) [1]	1280 × 720
South Hampton, NY (Shopping village) [7]	1920 × 1080
Oxford, UK (Street + sidewalk) [10]	1920 × 1080
South Hampton, NY (Traffic intersection) [14]	1920 × 1080

Table 1: **Summary of our video dataset.**

ing strategy in terms of (quickly) adapting to different query types, accuracy targets, objects of interest, and CNNs. As shown in Figure 8(top), the median discrepancy between each chunk’s ideal $max_distance$ value and that of the corresponding cluster centroid is only 0-8 frames; this jumps to 45-898 frames when comparing chunks with the centroid of the closest neighboring cluster. Figure 8(bottom) illustrates the importance of shrinking these discrepancies. More specifically, applying each centroid’s ideal $max_distance$ to all chunks in the corresponding cluster (i.e., Boggart’s approach) yields average accuracies that are consistently above the targets. The same is not true when using the ideal $max_distance$ values from the nearest neighboring cluster.

6 EVALUATION

We evaluated Boggart on a wide range of queries, CNNs, accuracy targets, and videos. Our key findings are:

- Boggart consistently meets accuracy targets while running the CNN on only 3-54% of frames, highlighting its model-agnostic ingest tasks and effective query-time adaptation.
- Boggart’s response times are 38-94% lower than No-Scope’s across all query types. Compared to Focus (which performs *model-specific* ingest processing), Boggart’s response times are 15% and 56% lower on counting and detection queries, and only 11% higher on classifications.
- Boggart’s ingest-time processing is 58% faster than Focus’, while also being model-agnostic and monetarily cheaper (Boggart uses only CPUs at ingest-time).
- Boggart’s ingest- and query-time tasks speed up nearly linearly with increasing compute resources.

6.1 Methodology

Video dataset. Table 1 summarizes the video sources used to evaluate Boggart. Our dataset considers 8 live-streaming cameras that cover diverse regions including traffic intersections, college campuses, town squares, and boardwalks. Video content across the cameras also varied in terms of resolution and camera orientation (relative to objects in the scene). From each camera, we scraped 12 hours of continuous video (at 30 fps) in order to capture varying levels of lighting and object densities (i.e., busyness).

Queries. We consider the three query types (and their corresponding accuracy definitions) described in §2.1, i.e., binary

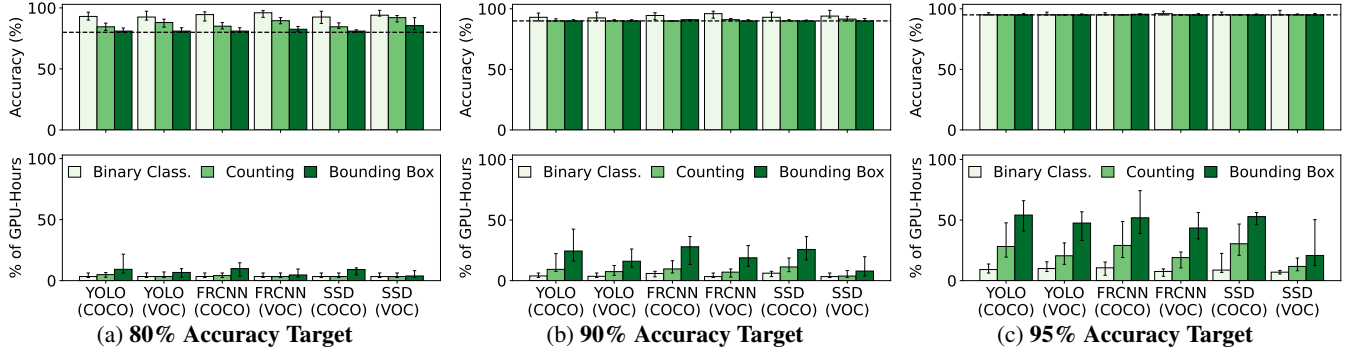


Figure 9: **Boggart’s query-time performance across a range of CNNs, query types, and accuracy targets; results are aggregated across object types.** Bars summarize the distributions of per-video average result accuracy (top) and percentage of GPU-hours required to generate results relative to running the CNN on all frames (bottom). Bars list medians with error bars spanning 25-75th percentiles.

classification, counting, and bounding box detection. For each type, we ran the query across our entire video dataset, and considered two objects of interest: people and cars. We evaluated Boggart with three accuracy targets – 80%, 90%, and 95% – and report accuracies as averages for each video.

CNN models. Since Boggart targets model-agnostic ingest-time speedups, our experiments cover a variety of CNNs. In particular, we consider three state-of-the-art and popular architectures (§2.3): (1) SSD with ResNet-50 as the base, (2) Faster RCNN with ResNet-50 as the base, and (3) YOLOv3 with Darknet53 as the base. For each, we used one version trained on the COCO dataset, and another trained on VOC Pascal. Trends for any results shown on a subset of CNNs (due to space constraints) hold for all considered models.

Hardware. Our experiments were run on a server with an NVIDIA GTX 1080 GPU (8 GB RAM) and an 18-core Intel Xeon Gold 5220 CPU (2.20 GHz; 125 GB RAM). The server ran Ubuntu 18.04.3 LTS.

Metrics. In addition to the accuracy of query results, we evaluate the query-time performance of all considered systems (Boggart, Focus [53], and NoScope [65]) in terms of the number of GPU-hours required to generate results. We report GPU-hours for two reasons: (1) CNN execution (on GPUs) accounts for almost all response generation delays with the baselines [53,65] and Boggart (§6.4), and (2) it is directly applicable to all of the systems, e.g., it incorporates NoScope’s specialized CNNs. For ingest-time, we report both GPU- and CPU-hours since Boggart only requires the latter. Note that, as in prior work [53,65], we exclude the video decoding costs that are shared (and unoptimized) by all considered systems.

6.2 End-to-End Performance

Figure 9 evaluates Boggart’s query-time performance across all combinations of the considered CNNs, query types, and accuracy targets. For context, performance results here are reported relative to a naive baseline that runs the CNN on all frames. Note that all of the results use the same outputs from Boggart’s model-agnostic ingest-time phase.

There are three points to take away from Figure 9. First,

Object Type →	People		Cars	
Query Type ↓	Acc.	% GPU-hrs	Acc.	% GPU-hrs
Binary Classif.	92%	6%	98%	3%
Counting	90%	11%	90%	7%
Bounding Box	91%	27%	90%	16%

Table 2: **Average accuracy and percentage of GPU-hours (relative to the naive baseline) for different query types and objects of interest. Results list median per-video values across all CNNs.**

across all of the conditions, Boggart *consistently* meets the specified accuracy targets. Second, the percentage of GPU-hours required to meet each accuracy target with Boggart grows as we move from coarse binary classification and counting queries (that require propagating object presence) to fine-grained bounding box detections (that require propagating precise object locations). For example, with a target accuracy of 90%, the median percentage of GPU-hours across all models was 3-6%, 4-11%, and 8-28% for binary classification, counting, and bounding box detections, respectively. Third, the percentage of GPU-hours also grows as the target accuracy increases for each query type. For instance, for counting queries, the percentage (across all CNNs) was 3-5% when the target accuracy was 80%; this jumps to 12-30% when the target accuracy grows to 95%. The reason is intuitive: higher accuracy targets imply that Boggart must more tightly bound the duration over which results are propagated (to limit propagation errors) by running the CNN on more frames. Note that Boggart’s speedups over the naive baseline are roughly equivalent to the percentage of frames on which Boggart ran the CNN in each case (§6.4).

Different object types. Table 2 reports the results from Figure 9 separately per object type (i.e., people and cars). As shown, the high-level trends from above persist for each. However, for a given query type, the percentage of required GPU-hours is consistently lower when considering cars versus people. The reason is twofold. First, inconsistencies in CNN results are more prevalent for people since, in our videos, they appear as smaller objects in the scene (§5.2). Second, cars are inherently more rigid than people, and thus deliver more stability in the anchor ratios that Boggart relies

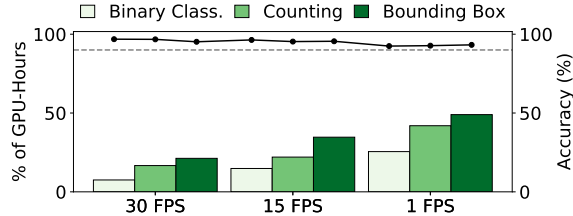
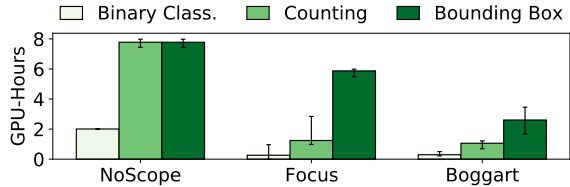
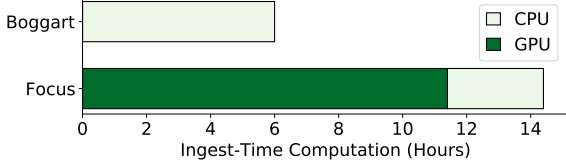


Figure 10: Average accuracy (line) and percentage of GPU hours (relative to the naive baseline) for different video sampling rates. Results are listed for the median video, and consider YOLOv3+COCO and a 90% accuracy target.



(a) Query-time efficiency. Bars list values for the median video, with error bars spanning 25-75th percentiles.



(b) Ingest-time efficiency. Bars list GPU/CPU-hours for the median video. NoScope does not perform ingest work.

Figure 11: Comparing Boggart, Focus [53], and NoScope [65]. Results use YOLOv3+COCO and a target accuracy of 90%.

on for bounding box propagation (§5.1); consequently, propagation errors for bounding box queries grow more quickly with people than with cars. Boggart handles both issues by running the CNN on more representative frames.

Downsampled video. To reduce costs or because only coarse results are required, users may issue queries on sampled versions of each video [53]. We evaluated Boggart with three different sample rates: 30 fps (default), 15 fps, and 1 fps. Although the number of considered frames drops, Figure 10 shows that Boggart’s query-time speedups persist when operating over downsampled videos. For instance, with 1-fps video, Boggart requires only 25-49% of the GPU-hours that the naive baseline would need across all query types. Figure 10 also shows that Boggart’s ability to consistently meet accuracy targets persists across all of the considered sampling rates. Digging deeper, we find that Boggart can hit its accuracy targets without resorting to running the CNN on all frames because object keypoints – the primitive that Boggart tracks across frames during both ingest-time trajectory construction and query-time detection propagation – typically persist across frames even at these sample rates. For instance, Boggart matches 85% of the median object’s keypoints across the 29-frame gap induced by the 1-fps rate.

6.3 Comparison to State-of-the-Art

We compared Boggart with two recent retrospective video analytics systems: (1) NoScope [65], a *query-time-only* accelerator that runs a cascade of specialized/compressed binary classification CNNs in place of the full CNN on most frames, and (2) Focus [53], a *model-specific ingest-time* accelerator that builds an approximate index of object appearances using a specialized/compressed CNN, clusters similar objects, and (at query-time) runs the full CNN on centroids (where the compressed CNN’s confidence was too low) to label all objects in each cluster. §2.1 details each system.

For these experiments, we set the query-time model to be YOLOv3+COCO, and the accuracy target to be 90%. Our Focus implementation used Tiny YOLO [84] as the specialized/compressed model, while NoScope used all of its open-source models. Following the training methodology used in both papers, we train the specialized/compressed models on 1-fps versions of the first half (i.e., 6 hours) of each video in our dataset, and run queries on the second half of each video.

Query-time. Figure 11a compares the query-time performance of all three systems. As shown, Focus requires 11% fewer median GPU-hours than Boggart for binary classification queries. The main reason is that Focus’ model-specific ingest-time clustering of objects enables more result propagation than Boggart’s model-agnostic trajectories, i.e., Focus can propagate labels across objects, whereas Boggart can propagate labels only along a given object’s trajectory (§3). In particular, median propagation distances for results from the full CNN are 58 and 44 frames with Focus and Boggart.

Summing Focus’ binary classifications to generate per-frame counts was insufficient for our 90% target. Thus, for counting queries, we performed favorable sampling until Focus hit 90% in each video: we greedily select a set of contiguous frames with constant count errors, run the CNN on a single frame, and correct errors on the remaining ones in the set. Even with such favorable sampling, Boggart required 15% fewer GPU-hours than Focus for counting queries.

Bounding box detections paint a starker contrast, with Boggart needing 56% fewer GPU-hours than Focus. Unlike with classification labels, Focus cannot propagate bounding boxes across frames. Instead, to accelerate these queries, Focus relies on binary classification, and runs the full CNN on all frames with an object of interest (to obtain their bounding boxes); for our videos, this translates to running the full CNN on 63-100% of frames. In contrast, Boggart propagates bounding boxes along each trajectory (median propagation distance of 23 frames) and reduces CNN tasks accordingly.

Compared to NoScope, Boggart’s query-time tasks consume 38-94% fewer GPU-hours across the three query types. Boggart’s speedups here are largely due to three reasons. First, NoScope does not perform ingest processing, and instead must train and run inference with its specialized/compressed CNNs at query-time. Second, results are not propagated across frames. Third, bounding box detections are sped

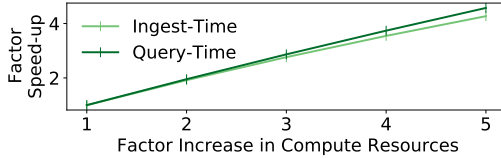


Figure 12: **Boggart’s performance with increasing compute resources.** Resource factors are multiples of the 18-core CPU and single GPU listed in §6.1. Results consider YOLOv3+COCO, a 90% accuracy target, and the median video.

up only via binary classification; note that NoScope performs binary classification on each frame (not object, like Focus), so counting queries cannot simply sum classification results per frame and instead are treated as bounding box queries.

Ingest-time. Figure 11b reports the ingest-time efficiency of all three systems. Since NoScope does not perform any ingest work, we center our discussion on Boggart and Focus. As shown, Boggart’s ingest-time tasks require 16% fewer computation hours than Focus’ tasks. Much like with NoScope’s query-time operation above, the discrepancy is driven by the training costs that Focus incurs for its specialized/compressed model at ingest-time, i.e., labeling the training dataset with the full CNN, and then training the smaller CNN. There are two important points to note when framing these results. First, *all* of Boggart’s ingest-time costs are CPU-based,² while Focus’ costs are dominated (79%) by (more monetarily expensive) GPU operations. Second, in practice, Boggart’s ingest-time tasks would be performed once per video, with the outputs being shared across all future CNNs. Focus, on the other hand, would have to perform all of its ingest-time work for each CNN that it wishes to support (to avoid the accuracy degradations described in §2.3).

6.4 Profiling Boggart

Dissecting Boggart’s performance. Boggart’s ingest delays are dominated (83% on the median video) by the extraction of SIFT keypoints across frames; background estimation, trajectory construction, and clustering together account for only 17% of the time. Query-time profiles are similar, with CNN inference on centroid chunks and representative frames contributing 7% and 91% of runtime; result propagation (mostly for detections) takes the remaining 2%.

Resource scaling. Figure 12 illustrates that Boggart’s ingest- and query-time performance scale nearly linearly with increasing CPU and GPU resources, respectively. The reason is that feature extraction and CNN inference, the tasks that (as noted above) dominate ingest/query-time delays, can naturally be parallelized across frames. Note that these results only parallelize tasks within each chunk (not across chunks).

Storage costs. Boggart’s ingest work generates 720 MB of data per 1 hour of video; for context, the video consumes 1 GB when encoded with H.264. Note that 98% of Boggart’s

storage overheads are for the keypoints used to propagate bounding boxes; blobs and trajectories consume only 2%.

Sensitivity to parameters. Boggart includes parameters for video chunk size (default: 1 min) and target number of clusters (default: centroids cover 2% of video). On average, we find that Boggart’s performance is largely insensitive to both: varying chunk sizes from 0.2-10 min and the videos covered by centroids from 0.5-5% altered Boggart’s performance by less than 5% (note that accuracy never dropped below the targets). However, the effects of each parameter are more pronounced on short amounts of video and are dependent on the content being considered. More specifically, smaller chunk sizes reduce the potential result propagation, but also shrink cluster centroids and increase the potential for parallel processing. Similarly, more clusters implies fewer suboptimalities in the selection of representative frames, but also additional centroids on which to run the CNN.

7 ADDITIONAL RELATED WORK

Live video analytics. Multiple systems accelerate queries on live video, with optimizations along the following axes: (1) profiling pipeline knobs to identify cheaper (but accurate) configurations [59, 101], (2) integrating on-camera or edge server resources for partial inference or filtering [31, 35, 41, 74, 92, 103], (3) content/model-aware encoding to reduce data transfers [40, 96], and (4) spatiotemporal coordination for efficient multi-camera queries [58, 79]. These systems share Boggart’s goals (i.e., low latency, high accuracy), but run over live video and with known CNNs, and thus face different challenges, e.g., load balancing, network delays.

Accelerating GPU tasks. One line of work optimizes DNNs for accelerated inference, either via distillation [51], quantization [37, 56, 105], or pruning [28, 77]. Another direction targets faster inference for a given model, either through better scheduling of GPU resources across inference tasks [57, 86, 90], or hardware acceleration [17, 43, 62, 82]. These works are complementary to Boggart, which focuses on reducing the number of frames on which inference must be performed.

Video Object Detection. In addition to those in §4, Boggart builds on a line of work in the CV community that aims to leverage the spatiotemporal aspect of video to accelerate detection and classification tasks. These techniques swap inference on sampled frames with optical flow networks that extend results from earlier frames [26, 32, 34, 36, 39, 48, 49, 69, 80, 93, 94, 106–108], and are thus similar in spirit to Boggart’s result propagation strategy. However, unlike Boggart, these approaches are model-specific, in that the networks used for propagation must be trained according to the specific CNN (e.g., its feature extractor) used for the target query.

Video storage and indexing. Many systems balance video storage and lookup costs for specific query types [85, 100, 104] or CNNs [19, 67, 83, 98]. Boggart is complementary to these works in that its focus is on performing model-agnostic

²Boggart could use GPUs to more quickly perform SIFT keypoint extraction [47], but we opt for CPUs to keep costs down.

ingest processing and accelerating response generation after video frames are loaded into memory.

8 CONCLUSION

Boggart accelerates retrospective video analytics by leveraging model-agnostic, traditional CV algorithms to perform ingest-time computations for a variety of query types. At query-time, Boggart employs a series of novel techniques to (1) efficiently discover and correct discrepancies between noisy ingest-time outputs and CNN results, and (2) accurately propagate sampled CNN results to the remaining frames. More broadly, we hope that our work inspires the judicious integration of CV algorithms into video analytics pipelines, not to replace highly accurate CNNs, but instead to carefully augment them for improved resource efficiency.

REFERENCES

- [1] 11 Street SW Calgary. <https://www.youtube.com/watch?v=iGxFLjqhKSA>.
- [2] Absolutely everywhere in beijing is now covered by police video surveillance. <https://qz.com/518874/>.
- [3] Are we ready for ai-powered security cameras? <https://thenewstack.io/are-we-ready-for-ai-powered-security-cameras/>.
- [4] British transport police: Cctv. http://www.btp.police.uk/advice_and_information/safety_on_and_near_the_railway/cctv.aspx.
- [5] Can 30,000 cameras help solve chicago's crime problem? <https://www.nytimes.com/2018/05/26/us/chicago-police-surveillance.html>.
- [6] City of Auburn Toomer's Corner Webcam 1. <https://www.youtube.com/watch?v=wVDtzDwo-1Q>.
- [7] Hamptons.com Southampton Village Cam, Hildreth's Home Goods LIVE. <https://www.youtube.com/watch?v=9IbruokZzx0>.
- [8] Jackson Hole Wyoming USA Town Square Live Cam. <https://www.youtube.com/watch?v=1EiC9bvVGnk>.
- [9] Lausanne, pont Bessières. <https://www.youtube.com/watch?v=TyElel0QjCI>.
- [10] Oxford Martin School Webcam - Broad Street, Oxford. <https://www.youtube.com/watch?v=St7aTfoldYQ>.
- [11] Paris hospitals to get 1,500 cctv cameras to combat violence against staff. <https://bit.ly/2OYiBz2>.
- [12] Powering the edge with ai in an iot world. <https://www.forbes.com/sites/forbestechcouncil/2020/04/06/powering-the-edge-with-ai-in-an-iot-world/>.
- [13] Resorts Casino Hotel Beach Camera. <https://www.youtube.com/watch?v=vVyBOU9Huvo>.
- [14] SouthHampton Traffic Cam. https://www.youtube.com/watch?v=Z9P_2pCgfBA.
- [15] Video analytics applications in retail - beyond security. <https://www.securityinformed.com/insights/co-2603-ga-co-2214-ga-co-1880-ga.16620.html/>.
- [16] The vision zero initiative. <http://www.visionzeroinitiative.com/>.
- [17] J. Albericio, A. Delmás, P. Judd, S. Sharify, G. O'Leary, R. Genov, and A. Moshovos. Bit-pragmatic deep neural network computing. In *Proceedings of the 50th Annual IEEE/ACM International Symposium on Microarchitecture, MICRO-50 '17*, page 382–394. Association for Computing Machinery, 2017.
- [18] Amazon. Rekognition. <https://aws.amazon.com/rekognition/>.
- [19] Amazon. AWS DeepLens. <https://aws.amazon.com/deeplens/>, 2019.
- [20] G. Ananthanarayanan, Y. Shu, M. Kasap, A. Kewalramani, M. Gada, and V. Bahl. Live video analytics with microsoft rocket for reducing edge compute costs, July 2020.
- [21] M. R. Anderson, M. J. Cafarella, G. Ros, and T. F. Wenisch. Physical representation-based predicate optimization for a visual analytics database. In *35th IEEE International Conference on Data Engineering, ICDE 2019, Macao, China, April 8-11, 2019*, pages 1466–1477, 2019.
- [22] M. Azure. Computer vision api. <https://azure.microsoft.com/en-us/services/cognitive-services/computer-vision/>, 2021.
- [23] M. Azure. Face api. <https://azure.microsoft.com/en-us/services/cognitive-services/face/>, 2021.
- [24] O. Barnich and M. Van Droogenbroeck. Vibe: A universal background subtraction algorithm for video sequences. *IEEE Transactions on Image processing*, 20(6):1709–1724, 2010.
- [25] F. Bastani, S. He, A. Balasingam, K. Gopalakrishnan, M. Alizadeh, H. Balakrishnan, M. Cafarella, T. Kraska, and S. Madden. Miris: Fast object track queries in video. In *Proceedings of the 2020 ACM SIGMOD International Conference on Management of Data, SIGMOD '20*, page 1907–1921. Association for Computing Machinery, 2020.
- [26] G. Bertasius, L. Torresani, and J. Shi. Object detection in video with spatiotemporal sampling networks. In *Proceedings of the European Conference on Computer Vision (ECCV)*, pages 331–346, 2018.
- [27] A. Bewley, Z. Ge, L. Ott, F. Ramos, and B. Upcroft. Simple online and realtime tracking. In *2016 IEEE international conference on image processing (ICIP)*, pages 3464–3468. IEEE, 2016.
- [28] D. Blalock, J. J. G. Ortiz, J. Frankle, and J. Gutttag. What is the state of neural network pruning? *arXiv preprint arXiv:2003.03033*, 2020.
- [29] S. Brutzer, B. Hoferlin, and G. Heidemann. Evaluation of background subtraction techniques for video surveillance. In *Proceedings of the 2011 IEEE Conference on Computer Vision and Pattern Recognition*,

- CVPR '11, pages 1937–1944, Washington, DC, USA, 2011. IEEE Computer Society.
- [30] Z. Cai, M. Saberian, and N. Vasconcelos. Learning complexity-aware cascades for deep pedestrian detection. In *Proceedings of the 2015 IEEE International Conference on Computer Vision (ICCV)*, ICCV '15, pages 3361–3369, Washington, DC, USA, 2015. IEEE Computer Society.
- [31] C. Canel, T. Kim, G. Zhou, C. Li, H. Lim, D. G. Andersen, M. Kaminsky, and S. R. Dulloor. Scaling video analytics on constrained edge nodes. In *2nd SysML Conference*, 2019.
- [32] Y. Chai. Patchwork: A patch-wise attention network for efficient object detection and segmentation in video streams. In *Proceedings of the IEEE/CVF International Conference on Computer Vision*, pages 3415–3424, 2019.
- [33] M.-C. Chang, Y. Wei, N. Song, and S. Lyu. Video analytics in smart transportation for the aic'18 challenge. In *Proceedings of the IEEE Conference on Computer Vision and Pattern Recognition (CVPR) Workshops*, June 2018.
- [34] K. Chen, J. Wang, S. Yang, X. Zhang, Y. Xiong, C. C. Loy, and D. Lin. Optimizing video object detection via a scale-time lattice. In *CVPR*, 2018.
- [35] T. Y.-H. Chen, L. Ravindranath, S. Deng, P. Bahl, and H. Balakrishnan. Glimpse: Continuous, real-time object recognition on mobile devices. In *Proceedings of the 13th ACM Conference on Embedded Networked Sensor Systems*, pages 155–168, 2015.
- [36] Y. Chen, Y. Cao, H. Hu, and L. Wang. Memory enhanced global-local aggregation for video object detection. In *Proceedings of the IEEE/CVF Conference on Computer Vision and Pattern Recognition*, pages 10337–10346, 2020.
- [37] M. Courbariaux, I. Hubara, D. Soudry, R. El-Yaniv, and Y. Bengio. Binarized neural networks: Training deep neural networks with weights and activations constrained to+ 1 or-1. *arXiv preprint arXiv:1602.02830*, 2016.
- [38] S. R. E. Datondji, Y. Dupuis, P. Subirats, and P. Vasseur. A survey of vision-based traffic monitoring of road intersections. *Trans. Intell. Transport. Sys.*, 17(10):2681–2698, Oct. 2016.
- [39] J. Deng, Y. Pan, T. Yao, W. Zhou, H. Li, and T. Mei. Relation distillation networks for video object detection. In *Proceedings of the IEEE/CVF International Conference on Computer Vision*, pages 7023–7032, 2019.
- [40] K. Du, A. Pervaiz, X. Yuan, A. Chowdhery, Q. Zhang, H. Hoffmann, and J. Jiang. Server-driven video streaming for deep learning inference. In *Proceedings of the Annual Conference of the ACM Special Interest Group on Data Communication on the Applications, Technologies, Architectures, and Protocols for Computer Communication*, SIGCOMM '20, page 557–570, New York, NY, USA, 2020. Association for Computing Machinery.
- [41] J. Emmons, S. Fouladi, G. Ananthanarayanan, S. Venkataraman, S. Savarese, and K. Winstein. Cracking open the dnn black-box: Video analytics with dnns across the camera-cloud boundary. In *Proceedings of the 2019 Workshop on Hot Topics in Video Analytics and Intelligent Edges*, HotEdgeVideo'19, pages 27–32, New York, NY, USA, 2019. Association for Computing Machinery.
- [42] M. Everingham, L. Gool, C. K. Williams, J. Winn, and A. Zisserman. The pascal visual object classes (voc) challenge. *Int. J. Comput. Vision*, 88(2):303–338, June 2010.
- [43] J. Fowers, K. Ovtcharov, M. Papamichael, T. Massengill, M. Liu, D. Lo, S. Alkalay, M. Haselman, L. Adams, M. Ghandi, S. Heil, P. Patel, A. Sapek, G. Weisz, L. Woods, S. Lanka, S. K. Reinhardt, A. M. Caulfield, E. S. Chung, and D. Burger. A configurable cloud-scale dnn processor for real-time ai. In *Proceedings of the 45th Annual International Symposium on Computer Architecture*, ISCA '18, page 1–14. IEEE Press, 2018.
- [44] Google. Cloud vision api. <https://cloud.google.com/vision>, 2021.
- [45] C. Grana, D. Borghesani, and R. Cucchiara. Optimized block-based connected components labeling with decision trees. *IEEE Transactions on Image Processing*, 19(6):1596–1609, 2010.
- [46] G. Grassi, K. Jamieson, P. Bahl, and G. Pau. Parkmaster: An in-vehicle, edge-based video analytics service for detecting open parking spaces in urban environments. In *Proceedings of the Second ACM/IEEE Symposium on Edge Computing*, SEC '17. Association for Computing Machinery, 2017.
- [47] C. Griwodz, L. Calvet, and P. Halvorsen. Popsift: a faithful sift implementation for real-time applications. In *Proceedings of the 9th ACM Multimedia Systems Conference*, pages 415–420, 2018.
- [48] C. Guo, B. Fan, J. Gu, Q. Zhang, S. Xiang, V. Prinet, and C. Pan. Progressive sparse local attention for video object detection. In *Proceedings of the IEEE/CVF International Conference on Computer Vision*, pages 3909–3918, 2019.
- [49] F. He, N. Gao, Q. Li, S. Du, X. Zhao, and K. Huang. Temporal context enhanced feature aggregation for video object detection. In *Proceedings of the AAAI Conference on Artificial Intelligence*, volume 34, pages 10941–10948, 2020.
- [50] K. He, G. Gkioxari, P. Dollár, and R. B. Girshick. Mask R-CNN. *CoRR*, abs/1703.06870, 2017.
- [51] G. Hinton, O. Vinyals, and J. Dean. Distilling

- the knowledge in a neural network. *arXiv preprint arXiv:1503.02531*, 2015.
- [52] D. Hoiem, Y. Chodpathumwan, and Q. Dai. Diagnosing error in object detectors. In *European conference on computer vision*, pages 340–353. Springer, 2012.
 - [53] K. Hsieh, G. Ananthanarayanan, P. Bodik, S. Venkataraman, P. Bahl, M. Philipose, P. B. Gibbons, and O. Mutlu. Focus: Querying large video datasets with low latency and low cost. In *13th USENIX Symposium on Operating Systems Design and Implementation (OSDI 18)*, pages 269–286, Carlsbad, CA, 2018. USENIX Association.
 - [54] J. Huang, V. Rathod, C. Sun, M. Zhu, A. Korattikara, A. Fathi, I. Fischer, Z. Wojna, Y. Song, S. Guadarrrama, and K. Murphy. Speed/accuracy trade-offs for modern convolutional object detectors. *CoRR*, abs/1611.10012, 2016.
 - [55] IBM. Maximo remote monitoring. <https://www.ibm.com/products/maximo/remote-monitoring>, 2021.
 - [56] B. Jacob, S. Kligys, B. Chen, M. Zhu, M. Tang, A. Howard, H. Adam, and D. Kalenichenko. Quantization and training of neural networks for efficient integer-arithmetic-only inference. In *Proceedings of the IEEE Conference on Computer Vision and Pattern Recognition*, pages 2704–2713, 2018.
 - [57] P. Jain, X. Mo, A. Jain, H. Subbaraj, R. S. Durani, A. Tumanov, J. Gonzalez, and I. Stoica. Dynamic space-time scheduling for gpu inference. *arXiv preprint arXiv:1901.00041*, 2018.
 - [58] S. Jain, X. Zhang, Y. Zhou, G. Ananthanarayanan, J. Jiang, Y. Shu, V. Bahl, and J. Gonzalez. Spatula: Efficient cross-camera video analytics on large camera networks. In *ACM/IEEE Symposium on Edge Computing (SEC 2020)*, November 2020.
 - [59] J. Jiang, G. Ananthanarayanan, P. Bodik, S. Sen, and I. Stoica. Chameleon: Scalable adaptation of video analytics. In *Proceedings of the 2018 Conference of the ACM Special Interest Group on Data Communication, SIGCOMM ’18*, pages 253–266, New York, NY, USA, 2018. ACM.
 - [60] J. Jodoin, G. Bilodeau, and N. Saunier. Urban tracker: Multiple object tracking in urban mixed traffic. In *IEEE Winter Conference on Applications of Computer Vision*, pages 885–892, 2014.
 - [61] J. Jodoin, G. Bilodeau, and N. Saunier. Tracking all road users at multimodal urban traffic intersections. *IEEE Transactions on Intelligent Transportation Systems*, 17(11):3241–3251, 2016.
 - [62] N. P. Jouppi, C. Young, N. Patil, D. Patterson, G. Agrawal, R. Bajwa, S. Bates, S. Bhatia, N. Boden, A. Borchers, R. Boyle, P.-I. Cantin, C. Chao, C. Clark, J. Coriell, M. Daley, M. Dau, J. Dean, B. Gelb, T. V. Ghaemmaghami, R. Gottipati, W. Gulland, R. Hagmann, C. R. Ho, D. Hogberg, J. Hu, R. Hundt, D. Hurt, J. Ibarz, A. Jaffey, A. Jaworski, A. Kaplan, H. Khaitan, D. Killebrew, A. Koch, N. Kumar, S. Lacy, J. Laudon, J. Law, D. Le, C. Leary, Z. Liu, K. Lucke, A. Lundin, G. MacKean, A. Maggiore, M. Mahony, K. Miller, R. Nagarajan, R. Narayanaswami, R. Ni, K. Nix, T. Norrie, M. Omernick, N. Penukonda, A. Phelps, J. Ross, M. Ross, A. Salek, E. Samadiani, C. Severn, G. Sizikov, M. Snellman, J. Souter, D. Steinberg, A. Swing, M. Tan, G. Thorson, B. Tian, H. Toma, E. Tuttle, V. Vasudevan, R. Walter, W. Wang, E. Wilcox, and D. H. Yoon. In-datacenter performance analysis of a tensor processing unit. *SIGARCH Comput. Archit. News*, 45(2):1–12, June 2017.
 - [63] D. Kang, P. Bailis, and M. Zaharia. Blazeit: Fast exploratory video queries using neural networks. *CoRR*, abs/1805.01046, 2018.
 - [64] D. Kang, P. Bailis, and M. Zaharia. Blazeit: Optimizing declarative aggregation and limit queries for neural network-based video analytics. *Proc. VLDB Endow.*, 13(4):533–546, Dec. 2019.
 - [65] D. Kang, J. Emmons, F. Abuzaid, P. Bailis, and M. Zaharia. Noscope: Optimizing neural network queries over video at scale. *Proc. VLDB Endow.*, 10(11):1586–1597, Aug. 2017.
 - [66] D. Kang, J. Guibas, P. Bailis, T. Hashimoto, and M. Zaharia. Task-agnostic indexes for deep learning-based queries over unstructured data, 2020.
 - [67] D. Kang, A. Mathur, T. Veeramacheneni, P. Bailis, and M. Zaharia. Jointly optimizing preprocessing and inference for dnn-based visual analytics. *Proc. VLDB Endow.*, 14(2):87–100, Oct. 2020.
 - [68] K. Kang, H. Li, J. Yan, X. Zeng, B. Yang, T. Xiao, C. Zhang, Z. Wang, R. Wang, X. Wang, and W. Ouyang. T-CNN: Tubelets With Convolutional Neural Networks for Object Detection From Videos. *IEEE Trans. Cir. and Sys. for Video Technol.*, 28(10):2896–2907, Oct. 2018.
 - [69] K. Kang, W. Ouyang, H. Li, and X. Wang. Object detection from video tubelets with convolutional neural networks. In *CVPR*, 2016.
 - [70] A. Krizhevsky, I. Sutskever, and G. E. Hinton. Imagenet classification with deep convolutional neural networks. *Commun. ACM*, 60(6):84–90, May 2017.
 - [71] B. Kueng, E. Mueggler, G. Gallego, and D. Scaramuzza. Low-latency visual odometry using event-based feature tracks. In *2016 IEEE/RSJ International Conference on Intelligent Robots and Systems (IROS)*, pages 16–23, Oct 2016.
 - [72] B. Laugraud, S. Piérard, and M. Van Droogenbroeck. Labgen: A method based on motion detection for generating the background of a scene. *Pattern Recognition Letters*, 96:12–21, 2017.
 - [73] H. Li, Z. Lin, X. Shen, J. Brandt, and G. Hua. A

- convolutional neural network cascade for face detection. In *2015 IEEE Conference on Computer Vision and Pattern Recognition (CVPR)*, pages 5325–5334, June 2015.
- [74] Y. Li, A. Padmanabhan, P. Zhao, Y. Wang, G. H. Xu, and R. Netravali. Reducto: On-Camera Filtering for Resource-Efficient Real-Time Video Analytics. *SIGCOMM '20*, page 359–376, New York, NY, USA, 2020. Association for Computing Machinery.
- [75] T. Lin, P. Dollár, R. Girshick, K. He, B. Hariharan, and S. Belongie. Feature pyramid networks for object detection. In *2017 IEEE Conference on Computer Vision and Pattern Recognition (CVPR)*, pages 936–944, July 2017.
- [76] X. Liu, P. Ghosh, O. Ulutan, B. S. Manjunath, K. Chan, and R. Govindan. Caesar: Cross-camera complex activity recognition. In *Proceedings of the 17th Conference on Embedded Networked Sensor Systems, SenSys '19*, page 232–244. Association for Computing Machinery, 2019.
- [77] Z. Liu, J. Li, Z. Shen, G. Huang, S. Yan, and C. Zhang. Learning efficient convolutional networks through network slimming. In *Proceedings of the IEEE International Conference on Computer Vision*, pages 2736–2744, 2017.
- [78] D. G. Lowe. Distinctive image features from scale-invariant keypoints. *Int. J. Comput. Vision*, 60(2):91–110, Nov. 2004.
- [79] Y. Lu, A. Chowdhery, and S. Kandula. Optasia: A relational platform for efficient large-scale video analytics. In *Proceedings of the Seventh ACM Symposium on Cloud Computing, SoCC '16*, pages 57–70, New York, NY, USA, 2016. ACM.
- [80] H. Mao, T. Kong, and W. J. Dally. Catdet: Cascaded tracked detector for efficient object detection from video. *arXiv preprint arXiv:1810.00434*, 2018.
- [81] OpenCV. Morphological Transformations. https://docs.opencv.org/master/d9/d61/tutorial_py_morphological_ops.html, 2020.
- [82] S. Park, J. Park, K. Bong, D. Shin, J. Lee, S. Choi, and H. Yoo. An energy-efficient and scalable deep learning/inference processor with tetra-parallel mimd architecture for big data applications. *IEEE Transactions on Biomedical Circuits and Systems*, 9(6):838–848, 2015.
- [83] A. Poms, W. Crichton, P. Hanrahan, and K. Fatahalian. Scanner: Efficient video analysis at scale. *ACM Trans. Graph.*, 37(4), July 2018.
- [84] J. Redmon and A. Farhadi. Yolov3: An incremental improvement. *arXiv preprint arXiv:1804.02767*, 2018.
- [85] W. Ren, S. Singh, M. Singh, and Y. S. Zhu. State-of-the-art on spatio-temporal information-based video retrieval. *Pattern Recogn.*, 42(2):267–282, Feb. 2009.
- [86] H. Shen, L. Chen, Y. Jin, L. Zhao, B. Kong, M. Philipose, A. Krishnamurthy, and R. Sundaram. Nexus: A gpu cluster engine for accelerating dnn-based video analysis. In *Proceedings of the 27th ACM Symposium on Operating Systems Principles, SOSP '19*, pages 322–337, New York, NY, USA, 2019. Association for Computing Machinery.
- [87] C. Stauffer and W. E. L. Grimson. Adaptive background mixture models for real-time tracking. In *Proceedings. 1999 IEEE Computer Society Conference on Computer Vision and Pattern Recognition (Cat. No PR00149)*, volume 2, pages 246–252 Vol. 2, 1999.
- [88] Y. Sun, X. Wang, and X. Tang. Deep convolutional network cascade for facial point detection. In *Proceedings of the 2013 IEEE Conference on Computer Vision and Pattern Recognition, CVPR '13*, pages 3476–3483, Washington, DC, USA, 2013. IEEE Computer Society.
- [89] Z. Tang, M. Naphade, M. Liu, X. Yang, S. Birchfield, S. Wang, R. Kumar, D. C. Anastasiu, and J. Hwang. Cityflow: A city-scale benchmark for multi-target multi-camera vehicle tracking and re-identification. *CoRR*, abs/1903.09254, 2019.
- [90] Y. Ukidave, X. Li, and D. Kaeli. Mystic: Predictive scheduling for gpu based cloud servers using machine learning. In *2016 IEEE International Parallel and Distributed Processing Symposium (IPDPS)*, pages 353–362. IEEE, 2016.
- [91] P. D. Z. Varcheie, M. Sills-Lavoie, and G.-A. Bilodeau. A multiscale region-based motion detection and background subtraction algorithm. *Sensors*, 10(2):1041–1061, 2010.
- [92] J. Wang, Z. Feng, Z. Chen, S. George, M. Bala, P. Pillai, S.-W. Yang, and M. Satyanarayanan. Bandwidth-efficient live video analytics for drones via edge computing. pages 159–173, 10 2018.
- [93] S. Wang, H. Lu, and Z. Deng. Fast object detection in compressed video. In *Proceedings of the IEEE/CVF International Conference on Computer Vision*, pages 7104–7113, 2019.
- [94] S. Wang, Y. Zhou, J. Yan, and Z. Deng. Fully motion-aware network for video object detection. In *Proceedings of the European conference on computer vision (ECCV)*, pages 542–557, 2018.
- [95] X. Wang, T. Xiao, Y. Jiang, S. Shao, J. Sun, and C. Shen. Repulsion loss: Detecting pedestrians in a crowd. In *Proceedings of the IEEE Conference on Computer Vision and Pattern Recognition*, pages 7774–7783, 2018.
- [96] Y. Wang, W. Wang, J. Zhang, J. Jiang, and K. Chen. Bridging the edge-cloud barrier for real-time advanced vision analytics. In *11th USENIX Workshop on Hot Topics in Cloud Computing (HotCloud 19)*, Renton, WA, July 2019. USENIX Association.

- [97] N. Wojke, A. Bewley, and D. Paulus. Simple online and realtime tracking with a deep association metric, 2017.
- [98] T. Xu, L. M. Botelho, and F. X. Lin. Vstore: A data store for analytics on large videos. In *Proceedings of the Fourteenth EuroSys Conference 2019*, EuroSys '19, pages 16:1–16:17, New York, NY, USA, 2019. ACM.
- [99] R. Yao, G. Lin, S. Xia, J. Zhao, and Y. Zhou. Video object segmentation and tracking: A survey. *ACM Trans. Intell. Syst. Technol.*, 11(4), May 2020.
- [100] J. Yuan, H. Wang, L. Xiao, W. Zheng, J. Li, F. Lin, and B. Zhang. A formal study of shot boundary detection. *IEEE Trans. Cir. and Sys. for Video Technol.*, 17(2):168–186, Feb. 2007.
- [101] H. Zhang, G. Ananthanarayanan, P. Bodik, M. Philipose, P. Bahl, and M. J. Freedman. Live video analytics at scale with approximation and delay-tolerance. In *Proceedings of the 14th USENIX Conference on Networked Systems Design and Implementation*, NSDI'17, pages 377–392, Berkeley, CA, USA, 2017. USENIX Association.
- [102] Q. Zhang, H. Sun, X. Wu, and H. Zhong. Edge video analytics for public safety: A review. *Proceedings of the IEEE*, 107(8):1675–1696, 2019.
- [103] T. Zhang, A. Chowdhery, P. Bahl, K. Jamieson, and S. Banerjee. The design and implementation of a wireless video surveillance system. pages 426–438, 09 2015.
- [104] X. Zhou, X. Zhou, L. Chen, and A. Bouguettaya. Efficient subsequence matching over large video databases. *The VLDB Journal*, 21(4):489–508, Aug. 2012.
- [105] C. Zhu, S. Han, H. Mao, and W. J. Dally. Trained ternary quantization. *arXiv preprint arXiv:1612.01064*, 2016.
- [106] X. Zhu, J. Dai, L. Yuan, and Y. Wei. Towards high performance video object detection. In *Proceedings of the IEEE Conference on Computer Vision and Pattern Recognition*, pages 7210–7218, 2018.
- [107] X. Zhu, Y. Wang, J. Dai, L. Yuan, and Y. Wei. Flow-guided feature aggregation for video object detection. In *Proceedings of the IEEE International Conference on Computer Vision*, pages 408–417, 2017.
- [108] X. Zhu, Y. Xiong, J. Dai, L. Yuan, and Y. Wei. Deep feature flow for video recognition. In *Proceedings of the IEEE conference on computer vision and pattern recognition*, pages 2349–2358, 2017.